JOURNAL OF MAGNETIC RESONANCE IMAGING 30:1012–1020 (2009)

**Original Research**

# Resovist Enhanced MR Imaging of the Liver: Does Quantitative Assessment Help in Focal Lesion Classification and Characterization?

Lucia Santoro, MD,[1] Luigi Grazioli, MD,[2] Antonella Filippone, MD,[3] Emanuele Grassedonio, MD,[4] Giacomo Belli, MS,[5] and Stefano Colagrande, MD[1]*

**Purpose:** To improve characterization of focal liver lesions by a prospective quantitative analysis of percentage signal intensity change, in dynamic and late phases after slow (0.5 mL/s) Resovist administration.

**Materials and Methods:** Seventy-three patients were submitted on clinical indication to MR examination with Resovist. Signal intensity of 92 detected focal lesions (5–80 mm) were measured with regions of interest and normalized to paravertebral muscle in arterial, portal, equilibrium and T1/T2 late phases, by two observers in conference. Five values of percentage variations per patient were obtained and statistically evaluated.

**Results:** The enhancement obtained on dynamic study is more suitable in hemangiomas and focal nodular hyperplasias than in adenomas and hepatocellular carcinomas. To discriminate benign versus malignant lesions on late-phase-T2-weighted images, a cutoff = −26%, allowed sensitivity and specificity values of 97.4% and 97.7%, respectively. Area under the receiver operating characteristic (ROC) curve was 0.99. To differentiate hemangioma versus all other focal liver lesions, on late-phase-T1-weighted images, a cutoff = +40% permitted sensitivity and specificity values of 90.5% and 98.0%, respectively. Area under the ROC curve was 0.98.

**Conclusion:** Late phase quantitative evaluation after slow Resovist administration, allows to differentiate malignant from benign hepatic masses and hemangiomas from all the others focal liver lesions, on T2-/T1-weighted acquisitions, respectively.

**Key Words:** focal liver lesions; Ferucarbotran; liver MRI; quantitative evaluation; Resovist; superparamagnetic iron oxide (SPIO)
**J. Magn. Reson. Imaging 2009;30:1012–1020.**


RESOVIST (SHU 555 A, Bayer Schering Pharma, Berlin, Germany) is a T2 superparamagnetic iron oxide (SPIO) contrast agent (CA). After intravenous administration, it is actively uptaken by cells of the reticuloendothelial system (RES) of the liver and spleen (1–3). As a consequence, Resovist was primarily used to improve focal liver lesion detection rate (4–7). Normal liver/splenic parenchyma and benign masses have a well represented RES and after SPIO administration signal intensity (SI) loss is detectable. Conversely, due to relative or absolute lack of RES, malignant lesions have no phagocytic capabilities, and do not change their SI in T2-weighted images, thus increasing conspicuity versus surrounding normal liver parenchyma.

Because the lesions T2 signal changes in proportion to Kupffer cell activity (8), some authors used SPIO to characterize focal liver lesions. Most have attempted a qualitative study (8–11), while only a few authors have adopted a quantitative analysis to improve characterization of metastases (12), hemangiomas (13), and focal liver lesions in general (14,15). The latter evaluation has been made only in the delayed RES specific phase without any information about dynamic T1 study.

SPIO also shows a T1 effect which is more relevant in a well hydrated environment, thus Resovist has also been used for T1-weighted imaging with vascular opacification and peculiar T1 enhancement of hemangiomas (14). Some authors (16,17) have reported dissatisfaction with SPIO arterial phase after bolus injection in clinical practice. A new protocol has been proposed to improve the enhancement in dynamic

[1]Dipartimento di Fisiopatologia Clinica, Sezione di Radiodiagnostica, Università degli Studi di Firenze, Azienda Ospedaliero-Universitaria Careggi, Firenze, Italia.
[2]Dipartimento di Radiologia, Azienda Ospedaliera Spedali Civili Brescia Piazzale Spedali Civili, Brescia, Italia.
[3]Dipartimento di Scienze Cliniche e Bioimmagini, Sezione di Scienze Radiologiche "G. d'Annunzio" University of Chieti, "SS. Annunziata" Hospital Chieti, Italia.
[4]Dipartimento di Biotecnologie Mediche e Medicina Legale (DI.BI.ME.L.), Sezione di Scienze Radiologiche, Policlinico Universitario Paolo Giaccone, Università degli Studi di Palermo, Palermo, Italia.
[5]Struttura Organizzativa Dipartimentale Fisica Sanitaria, Azienda Ospedaliero-Universitaria Careggi, Firenze, Italia.
*Address reprint requests to: S.C., Sezione di Radiodiagnostica, Dipartimento di Fisiopatologia Clinica, Università degli Studi di Firenze, Azienda Ospedaliero-Universitaria di Careggi, Viale Morgagni 85, 50134 Firenze, Italy. E-mail: stefano.colagrande@unifi.it
Received May 25, 2009; Accepted August 7, 2009.
DOI 10.1002/jmri.21937
Published online in Wiley InterScience (www.interscience.wiley.com).

Table 1
Case Distribution and Diagnosis

| 92 Lesions (73 patients) | Diagnosis (patients) |
|---|---|
| 21 Hemangiomas (16) | At least 1 year MR follow-up (16) |
| 10 Adenomas (4) | Gadolinium BOPTA MR and biopsy (4) |
| 18 FNHs (15) | Gadolinium BOPTA MR (15) |
| 8 HCCs (7) | Barcelona 2005 criteria (4) and biopsy (3) |
| 35 Metastases (31) | Clinical/imaging follow-up (16) and biopsy (15) |

phase (at the rate of 0.5 mL/s against the usual rate of 2 mL/s) (18).

The aim of this prospective study was to improve the classification (i.e., attribution to a benign or malignant class) and characterization of the most frequent focal liver lesions, by a simple quantitative analysis of percentage signal intensity changes achievable during routine acquisitions, in dynamic and delayed phases, after slow Resovist administration.

## MATERIALS AND METHODS

### *Study Population*

From March 2007 to November 2008, 80 patients were enrolled for MRI with Resovist. The inclusion criteria were as follows: of-age patients, routinely referred for MR to follow up known benign focal liver lesion(s) or to confirm malignant mass(es) already detected with previous CT; no more than three lesions; no moderate to severe steatosis diagnosed by visual grading criterion (19). Of the 80 patients enrolled, 2 refused MR examination (claustrophobia) and 1 declined administration of CA. Resovist-enhanced MR imaging could not be completed in two patients because of slight adverse reactions immediately after infusion of the CA; two patients were excluded for technical reasons (respiratory artifacts). The final study group included 73 patients (29 males and 44 females; mean age, 54 ± 15 years; range, 24–82 years) with a total amount of 92 lesions, ranging in diameter from 5 to 80 mm (mean, 28.48 ± 17.44). Patient diagnosis was provided by combined clinical, imaging, laboratory and pathological findings (Table 1). Four patients presented with 3 lesions, 12 with 2 lesions (among these, 2 patients had two different types of lesions: 1 hemangioma and 1 metastasis; 1 focal nodular hyperplasia [FNH] and 1 adenoma), while remaining 56 showed only one nodule. Liver metastases arose from the following primary tumors: breast cancer (10 patients), colorectal (10 patients), lung (3 patients), pancreatic (2 patients), gastric (2 patients), larynx, carcinoid tumor, gastrointestinal stromal tumor, unknown origin (1 patient).

To obtain data about normal liver parenchyma, we evaluated 28 subjects (7 males and 21 females; mean age, 50 ± 15 years; range, 26–80 years) undergoing MR examination with Resovist to study splenic pathology (focal lesions in normal sized spleen); these patients had no clinical and/or imaging signs of liver pathology. All examinations were carried out for clinical indications and patients, after being informed about possible risks of intense magnetic field exposure and contrast medium injection, gave their written consent. Ethical committee approval and patient permission were not required for this prospective study, as patient privacy was maintained and patient care was not affected. All the lesions had already been detected and the purpose of the MR examination was to evaluate possible change in dimensions, number of benign masses or to confirm the presence of malignancy. All data and information derived from and pertaining to the study were under the exclusive control of the investigating radiologists.

### *MR Imaging Protocol*

All MR examinations were performed using a 1.5 Tesla (T) imaging system (Symphony, TIM Class, Siemens, Erlangen, Germany) equipped with a four-channel phased array multicoil, adequately positioned to cover the upper abdomen of the patient lying in a supine position. The scanner provides a maximum gradient strength of 30 mT/m, with a peak slew rate of 120 mT/m/ms. The baseline MRI protocol included the following transverse acquisitions:

(1) T2-weighted half-Fourier single-shot turbo spin-echo (HASTE) free-breath sequence: repetition time/echo time (TR/TE) = 8/79 ms, echo-train length = 90, slice thickness = 5 mm, intersection gap = 10%, field of view (FOV) = 350–400 mm, effective matrix size = 256 × 165, number signal averages (NSA) = 1, acquisition time = 2–3 min;

(2) T1-weighted 3D-GRE with volumetric interpolated breath-hold examination (VIBE) fat sat sequence: TR/TE = 3.8/1.5 ms, slice thickness = 4 mm, intersection gap = 10%, flip angle = 80°, FOV = 350–400 mm, effective matrix size = 256 × 169, parallel imaging reduction factor = 2, NSA = 1, acquisition time = 16 s. This sequence includes a sequential phase-encode order in the $k_y$ direction and a centric phase-encode reordering in the $k_z$ direction (partitions loop) to optimize fat-saturation uniformity.

After CA administration, the 3D sequence was repeated during hepatic artery phase (HAP) with a delay determined by Care Bolus technique. The acquisition was repeated again at 75 s during portal vein phase (PVP), at 180 s during equilibrium phase (EP) and at 10 min in late phase (LP). The HASTE sequence was repeated during the LP.

The Care Bolus technique in the sagittal and parasagittal orientations was used to determine the exact time to begin the artery phase acquisition, considering one scan per second: TR/TE = 3.5/1.1 ms, slice thickness = 60 mm, intersection gap = 20%, FOV = 400 mm, effective matrix size = 128 × 128, NSA = 2. The region of interest (ROI) with appropriate size was located in the abdominal aorta at the level of the celiac trunk. The Care Bolus reached the ROI level after 20–30 s, on the average; we began the GRE-3D VIBE sequence acquisition with a further delay of 10 s, and then after 30–40 s from the beginning of the CA

administration, by an automatic breath-hold (expiratory) recorded voice command (given 6 s in advance to the start of the acquisition).

Resovist was administered in a bolus by prefilled syringe (dose 0.9 mL in patients with a body weight lower than 60 kg, and 1.4 mL higher than 60 kg) in the distal part of a connecting line into an antecubital vein, followed by flushing with 20 mL of saline solution using an automated injector (Spectris Solaris EP, MedRad, Indianola, PA), at the rate of 0.5 mL/s to obtain a wider window of enhancement (18). The duration of the entire administration (CA plus 20 mL saline flush) was approximately 40–42 s. To avoid too great a difference in the administered CA quantity among various sized patients, we adopted an empirical rule, limiting the dose to 1.2 mL until the weight of 75 kg. So the range was from 0.015 to 0.018 mL of CA per kg of body weight for patients ranging from 50 to 90 kg, that is 0.9 mL $<$ 60 kg, 1.2 mL from 60 to 75 kg, 1.4 mL $>$ 75 kg. Patients were monitored for 2 h after the examination for adverse effects.

### *Image Analysis*

SIs of normal liver parenchyma and hepatic lesions were measured and normalized to paravertebral muscle for each patient before and after injection of CA in HAP, PVP, EP, LP, T1- and T2-weighted. Each SI reading was obtained in conference by two observers with ROIs placed as described below, and disagreements were resolved by consensus. Because of minimum changes in the position of the patients during examinations, pre and post SHU-555A ROIs were manually defined on each image as much reproducibly as possible. A ROI of 400 $mm^2$ was used to measure the SI of the healthy liver parenchyma; ROIs were placed to avoid large blood vessels, boards and artifacts, so that standard deviations (SDs) were no higher than 10%. According to nodular size, the largest ROIs were used to measure the SI of focal lesions; ROIs were placed to avoid necrosis and scarring within the nodular masses, so that SDs were always no higher than 20%. SIs were measured in each sequence and to avoid rescaling phenomenon, were normalized to paravertebral muscle SIs.

Percentage signal intensity change (PSIC) was calculated as: [(SI post-CA – SI pre-CA/ SI pre-CA) $\times$100] and was normalized (NPSIC) to paravertebral muscle SI using the following formula: NPSIC (in percent) = [(SI post-CA / SI pre-CA) $\times$ (N pre-CA / N post-CA) –1] $\times$100.

We obtained 5 NPSIC evaluations (five values of percentage variations) per patient: T1-weighted HAP, PVP, EP, LP, T2-weighted LP. Every quantitative evaluation was decided in conference by the two main investigators, both with more than 15 years of experience in liver MR imaging and 5 years in imaging with SPIO; conflicts were resolved by consensus.

### *Statistical analysis*

Statistical evaluations were performed using the SPSS package version 12 (SPSS Inc., Chicago, IL). Data are expressed and were analyzed as groups of lesions and as individual lesions.

#### *Group Analysis*

We reported mean $\pm$ standard deviation in all phases; SIs in the liver and hepatic lesions before and after SHU-555A were evaluated to find any significant difference. Normalized SIs for normal liver parenchyma and all lesions, within each group (normal liver, FNH, hemangioma, hepatocellular carcinoma [HCC], metastasis, adenoma), were tested using the Student paired t-test for significance at a level $P < 0.01$. Statistical analysis of NPSICs mean values for all groups (liver and focal lesions) was performed by analysis of variance test. It followed a post hoc comparison (Tamhane test) to find out which groups were significantly different from each other and which were not.

#### *Individual Analysis*

We used scatter plot representation. Using our best results (to classify/characterize focal liver lesions) we constructed a receiver operating characteristic (ROC) curve to determine the point nearest to the upper left corner, corresponding to the best sensitivity and specificity couple of the test; the area under the curve was also calculated. Logistic regression preanalysis was made.

## RESULTS

Two patients experienced slight adverse reactions (itch and flushing with facial and neck erythema, conjunctivitis) which disappeared without any therapy in approximately 5 min; however, the examinations were completed without early contrastographic phases and these patients were not included in the study group.

### *Group Results*

Mean SI $\pm$ SD and statistically significant SI differences are shown (Table 2). NPSIC values of each class (normal liver, adenoma, hemangioma, FNH, HCC, and metastasis) in all phases are detailed (Table 3) (Fig. 1). On T2-weighted images, Student paired t-test was statistically significant for liver, FNH, adenoma and hemangiomas before and after CA administration, at the sole late acquisitions (Fig. 2). Conversely, no statistically significant SI changes for metastases and HCCs were observed at the same comparison. T1-weighted images had statistically significant SI change only for hemangiomas in dynamic and late phases, for FNH in dynamic phases, and for liver in arterial and portal phases (Table 2) (Fig. 3). On T2-weighted LP sequence, NPSIC mean values were significantly different (Tamhane test) in normal liver and benign lesions versus malignant masses; no significant difference was found between normal liver and benign lesions. On T1-weighted HAP sequence, FNHs were significantly different from metastases. On T1-weighted PVP hemangiomas were significantly different from all others except FNHs; on T1-weighted EP

Table 2
Normalized Signal Intensity Mean Value*

| | Unenhanced phase | | Enhanced phases | | | | |
|---|---|---|---|---|---|---|---|
| Signal intensity | T2-weighted | T1-weighted | Arterial | Portal venous | Equilibrium | Delayed phase T1 | Delayed phase T2 |
| Liver | 1.19 ± 0.5 | 1.27 ± 0.4 | 1.38 ± 0.44* | 1.43 ± 0.45* | 1.35 ± 0.44 | 1.18 ± 0.44 | 0.5 ± 0.22* |
| Hemangiomas | 2.7 ± 1.75 | 0.85 ± 0.37 | 1.18 ± 0.66* | 1.38 ± 0.71* | 1.45 ± 0.67* | 1.47 ± 0.61* | 1.39 ± 1.09* |
| Adenomas | 1.48 ± 0.44 | 1.39 ± 0.53 | 1.42 ± 0.36 | 1.39 ± 0.43 | 1.54 ± 0.69 | 1.35 ± 0.45 | 0.83 ± 0.26* |
| FNHs | 1.69 ± 0.66 | 1.01 ± 0.34 | 1.23 ± 0.43* | 1.18 ± 0.41* | 1.09 ± 0.38* | 1 ± 0.35 | 0.93 ± 0.51* |
| HCCs | 1.16 ± 0.57 | 0.57 ± 0.20 | 0.66 ± 0.21 | 0.65 ± 0.23 | 0.61 ± 0.23 | 0.61 ± 0.19 | 1.17 ± 0.52 |
| Metastases | 1.48 ± 1.04 | 0.76 ± 0.49 | 0.74 ± 0.42 | 0.75 ± 0.42 | 0.74 ± 0.47 | 0.79 ± 0.49 | 1.46 ± 1.01 |

*Data are means ± standard deviation. When asterisk (*) is present, the difference of signal intensity between pre-SPIO and post-SPIO administration was statistically significant ($P < 0.01$).

and LP sequence, hemangiomas were significantly different from all others (Table 3). The most relevant results for classifying focal liver lesions were observed at T2 and T1-weighted LP acquisitions (Table 2). T2 NPSIC ranged from −22 to −73, mean −43 ± 13 for benign lesions, and from −22 to +58 mean +1 ± 18, for malignant lesions; the difference between benign/malignant groups was statistically significant ($P < 0.01$). T1-weighted NPSIC were always higher than +19 for hemangiomas and always lower than +60 for other lesions; the difference between the hemangioma/nonhemangioma groups was statistically significant ($P < 0.01$) (Figs. 2–5).

### *Individual Results*

On the basis of group results, we report in a scatter plot (as individual values) only T2 and T1-weighted LP NPSIC values for each lesion, to show different distribution for benign versus malignant lesions (Fig. 6) and for hemangioma versus nonhemangioma (Fig. 7). Logistic regression performed on these values confirmed the hypothesis of significant dependence between NPSIC and malignant status, on T2-weighted LP images ($P = 0.004$); between NPSIC and hemangiomas status, on T1-weighted LP images ($P = 0.0001$). ROC analysis gave us evidence for several sensitivity and specificity values versus NPSIC.

To distinguish between benign versus malignant lesions on T2-weighted images, a cutoff = −26% allowed 97.4% sensitivity and 97.7% specificity. Area under the ROC curve was 0.99. Two false positives, represented by one FNH and one adenoma, and one false negative due to well differentiated HCC, were found (Fig. 6).

To distinguish hemangioma from all other focal liver lesions on T1-weighted images, a cutoff = +40% permitted 90.5% sensitivity and 98.0% specificity. Area under the ROC curve was 0.98. Two false positives, represented by one FNH (not the same as reported above) and one metastasis, and two false negatives due to hemangiomas (6- and 8-mm diameter) were detected (Fig. 7).

## DISCUSSION

Quantitative evaluation of enhancement induced by slow SHU-555A administration allowed us to differentiate benign (hemangiomas, adenomas, and FNHs) from malignant (HCCs and metastases) lesions on T2-weighted late phase images in our patients with a cutoff = −26%, 97.4% sensitivity and 97.7% specificity (Fig. 6). On T1-weighted late phase images, a cutoff = +40% differentiated hemangiomas from all other focal liver lesions with 90.5% sensitivity and 98.0% specificity (Fig. 7).

In the analysis of groups of lesions, hemangiomas were significantly different from all other lesions also on T1-weighted EP sequence. Finally, dynamic study with slow bolus demonstrated statistically significant SI change versus unenhanced scan for liver, FNH, hemangioma (in HAP and PVP), and hemangiomas and FNHs (in EP) (Fig. 1; Tables 2 and 3). Resovist with slow bolus provided a suitable dynamic study of hemangiomas (Fig. 3) and FNHs. On the contrary, adenomas and HCCs (Fig. 5) were not significantly enhanced at dynamic study. In only three cases (2 adenomas and 1 HCC, and then 3 lesions out of 18) was valid enhancement on HAP detected (Fig. 2). This last finding is in contrast with a prior study with slow bolus Resovist administration, where the best enhancement achievable did not seem related to a particular category of focal lesion and was appreciable in all histological types with the same evidence (18).

Table 3
Normalized Percentage Signal Intensity Change (NPSIC)*

| NPSIC % | Arterial | Portal venous | Equilibrium | Delayed phase T1 | Delayed phase T2 |
|---|---|---|---|---|---|
| Liver | 9 ± 10 | 13 ± 11 | 7 ± 12 | −6 ± 15 | −56 ± 10 |
| Hemangiomas | 36 ± 47 | 63 ± 52 | 74 ± 43 | 78 ± 34 | −50 ± 13 |
| Adenomas | 8 ± 20 | 5 ± 21 | 9 ± 15 | −1 ± 7 | −43 ± 10 |
| FNHs | 23 ± 16 | 17 ± 13 | 8 ± 15 | 2 ± 20 | −44 ± 14 |
| HCCs | 5 ± 10 | 9 ± 12 | 6 ± 10 | 12 ± 14 | −1 ± 21 |
| Metastases | 2 ± 22 | 2 ± 20 | −3 ± 13 | 6 ± 17 | 2 ± 18 |

*Data are means ± standard deviation.

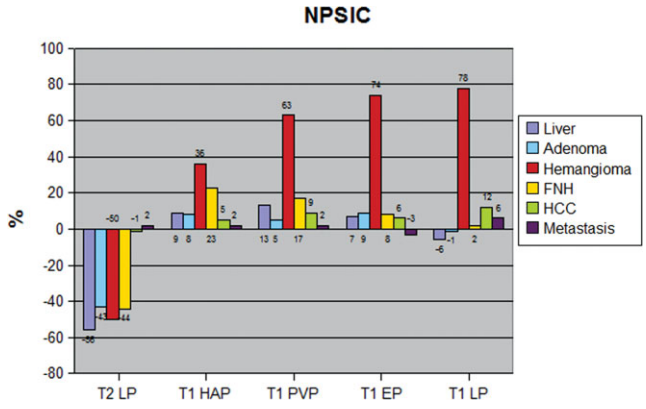


**Figure 1.** Graph-Normalized Percentage Signal Intensity Change (NPSIC). Enhancement values of each class (normal liver, adenoma, hemangioma, FNH, HCC, and metastasis) are graphically represented in all acquisition phases.

However, the previous experience was performed with a qualitative approach, and we believe that lesion changes are more appreciable by quantitative evaluation, which is easy and rapid to obtain by the proposed method, rather than by visual qualitative evaluation which often misjudges the enhancement, in particular on the T2-weighted acquisition, in our opinion because of the strong rescaling phenomenon induced by Resovist administration (Figs. 2, 4, 5). In our series, the rescaling bias was avoided by introduction of the normalization factor (a muscular structure of the back). One possible explanation for the different contrastographic features identified may be due to the typical enhancement of hemangiomas and FNHs during dynamic acquisition, usually less transient than the enhancement shown in adenomas and HCCs. Generally, we can confirm the minor conspicuity upon dynamic evaluation of hypervascular lesions after Resovist administration versus gadolinium chelates CA, despite the adoption of the slow infusion protocol, noted in a prior study (18).

In our analysis, with the given cutoff, we found in T2-weighted LP values, two false positives (one FNH, one adenoma) and one false negative (one HCC) (Fig. 6). The FNH had a large T2-hyperintense scar, which we presume contained a lower quantity of RES and then minor CA phagocytosis, thus explaining the

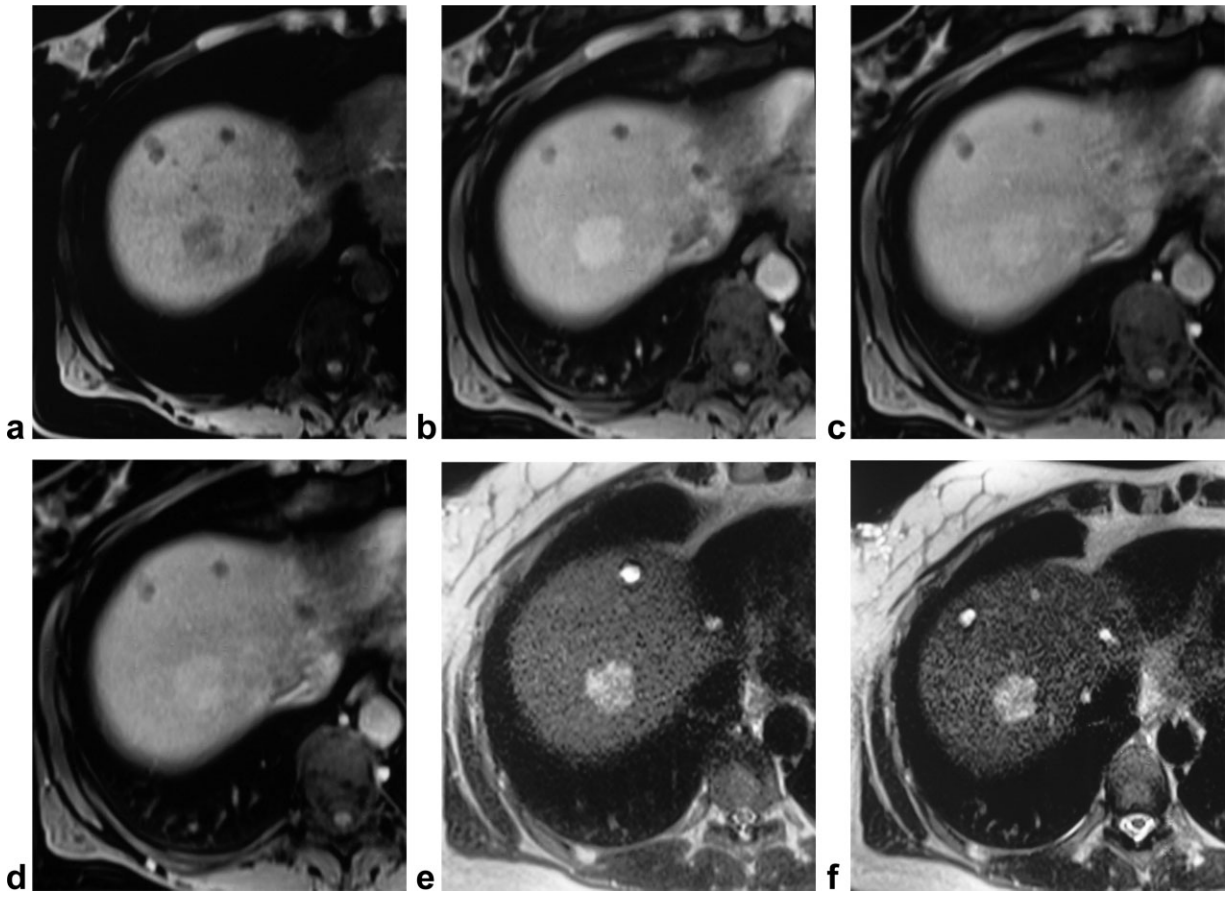


**Figure 2. a–f:** Hepatic adenoma. On the unenhanced T1-weighted VIBE acquisition (a) a nodule heterogeneously hypointense versus surrounding right liver lobe parenchyma, is detectable. After slow bolus Resovist administration nodule enhances in the arterial phase (b), without any appreciable wash-out during portal venous (c) and equilibrium phases (d). On the unenhanced HASTE T2-weighted sequence (e), the lesion appears hyperintense versus liver parenchyma, without any significant changes on the 10-min contrast-enhanced acquisition (f), at visual assessment. However, the quantitative analysis demonstrated a −33% signal loss of the nodule which appears still hyperintense due to a −53% signal loss of the surrounding parenchyma. Note, in all the images (a–f), some little cysts in the anterior portion of the liver parenchyma.

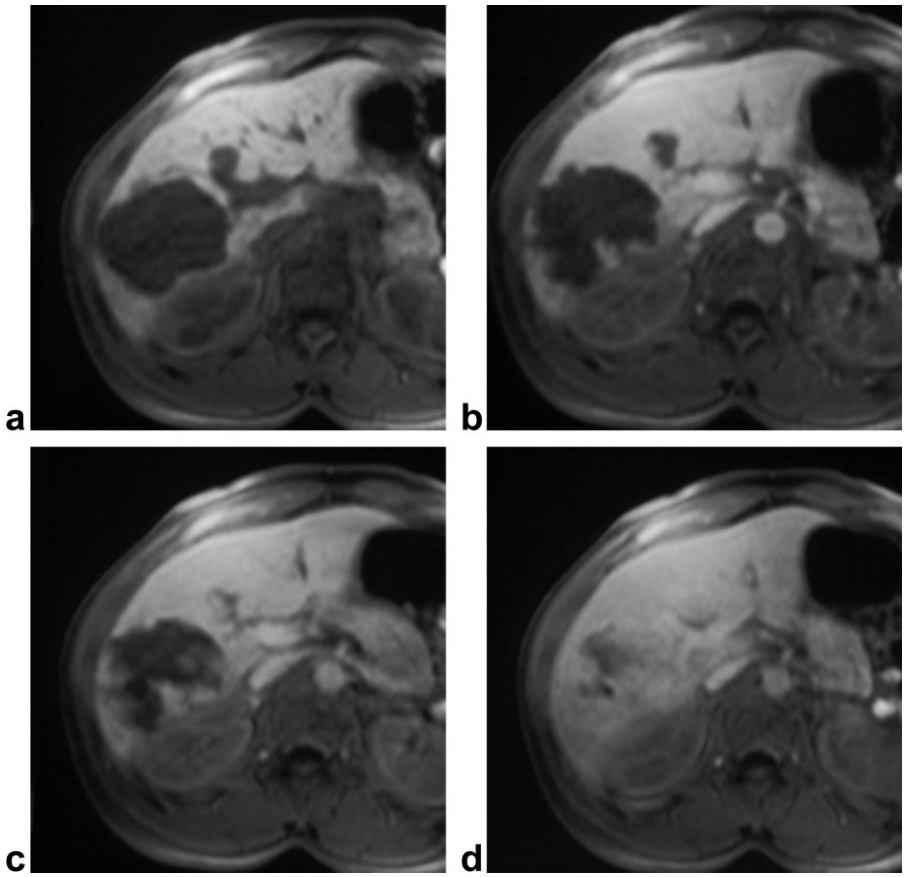


**Figure 3. a–d:** Hepatic hemangioma. On the unenhanced T1-weighted VIBE acquisition (a), a large nodule hypointense versus surrounding right liver lobe parenchyma, is appreciable. After slow bolus Resovist administration, nodule shows a slow fill-in phenomenon in the arterial and equilibrium phases (b,c), becoming almost isointense versus surrounding parenchyma on the 10-min T1-weighted acquisition (d).

slight SI loss. We hypothesize the same reason for the adenoma, which is well known to have a variable amount of RES. On the contrary, the HCC was a well differentiated type, which usually maintains a normal amount of RES.

In T1-weighted LP values analysis, two false positives (one FNH, one metastasis) and two false negatives (two hemangiomas) were found (Fig. 7). FNH showed a hyperintense scar at 90-min acquisition after liver specific gadolinium chelates administration and so we believed this scar was rich in soft interstitial tissue. Metastasis was hypervascular (from carcinoid tumor). In both cases, we suppose there was a trapping phenomenon similar to that which explains late hyperintensity of hemangiomas: we mean that the particles of CA enter the pathological vessels of the hypervascular nodule and the lacunae of the hemangiomas, they cluster and remain into vascular spaces, lacking the effect of the RES. Either the first or the second nodule was appropriately classified as benign and malignant, respectively, on the basis of their T2 patterns. In the case of metastasis it is probable that trapping was sufficient to determine the T1 enhancement but not to induce a significant T2 signal loss. Both hemangiomas presented a great signal loss in T2-weighted acquisition. This has led us to believe that a significant trapping effect with SPIO particles cluster occurred in these hemangiomas, determining an important signal decrease both in T2 and T1-weighted sequences. Moreover these hemangiomas had very small dimension, so we believe the minor SI measured, was also due to a partial volume effect. On the whole, the total amount of errors in characterization was only due to T2 false positives in 3 out of 92 lesions (3.26%).

There are other quantitative studies regarding the use of the SPIO CA to improve characterization of metastases (12), hemangiomas (13), and various focal liver lesions (14,15) in the literature. Only the latter proposed a quantitative characterization in a large series of different focal liver lesions; however, unlike our study, these authors carried out the quantitative study only in the late T2-weighted phase and without signal normalization. Other authors (13,14) normalized SI to the muscle, but the adoption of Endorem (ferumoxide, Guerbet, Aulnay-sous-Bois, France) did not allow them to perform the dynamic study. According to our results, these authors found no significant SI change in T2-weighted acquisitions for metastases (12) and HCCs (13,15), and confirmed significant SI loss for FNHs (13–15), hemangiomas (13–15), and adenomas (14,15). T1-weighted late phase study results are similar for hemangiomas as well (13,14). Chen et al compared Endorem and Resovist by a quantitative analysis of liver/spleen parenchyma and liver metastases with results analogous to ours for liver parenchyma and metastases, both in T2 and T1-weighted sequences. However, the studies are quite dissimilar because they administered Resovist in a rapid bolus and studied secondary tumors only, while we did not evaluate the spleen.

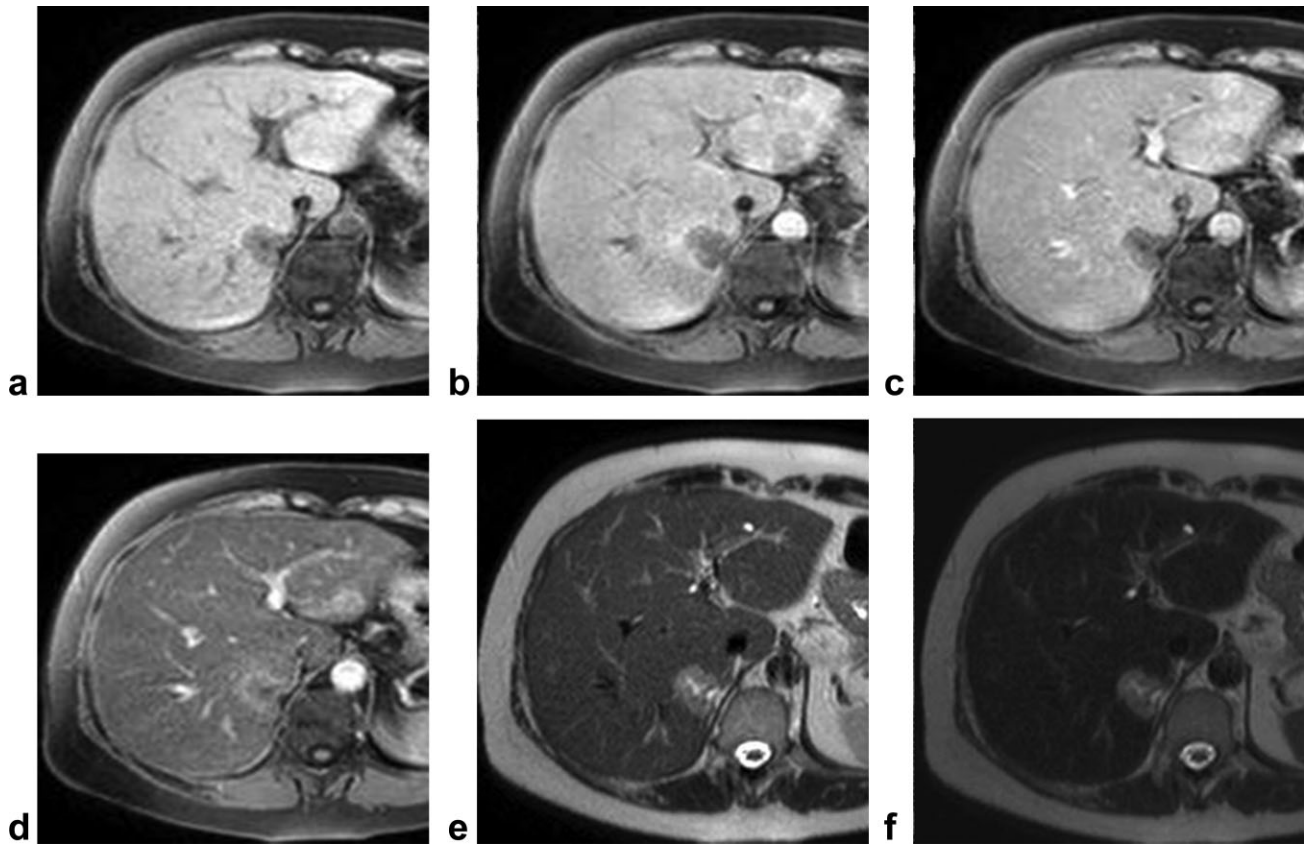


**Figure 4. a–f:** Liver metastasis (from colon cancer). On the unenhanced T1-weighted VIBE acquisition, in the medial part of the VII segment, a nodule hypointense versus surrounding parenchyma, is visible (a). After slow bolus Resovist administration, no enhancement can be detected on the arterial and portal phases (b,c), while on the 10-min T1 image (d) a peripheral ring of enhancement due to the compressed adjacent liver parenchyma, is demonstrable. On the unenhanced HASTE T2-weighted sequence (e), the lesion appears hyperintense versus liver parenchyma, with central necrotic scar. No signal intensity change, also at quantitative analysis, is demonstrable on the 10-min contrast-enhanced acquisition (f), where the nodule appears more hyperintense due to the signal decrease of the normal parenchyma.

So we can affirm that our work could be of some interest and novelty because we used (i) a quantitative rather than qualitative approach, (ii) a slow bolus administration, (iii) normalization with paravertebral muscle, and (iv) a large series of different focal liver lesions. Nevertheless, our study has two main limitations, as well.

First, the number of studied lesions is small, due to the interruption of the trial because in our country distribution of Resovist was stopped at the end of 2008. However, each class of the more frequent masses is represented and our results can at least provide an indication of the performance achieved by the described quantitative method.

Second, we did not perform the evaluation with the T2*-weighted gradient-echo sequences. Whether the latter sequence or T2-weighted fast spin-echo images are superior in the liver-specific phase of SPIO-enhanced liver MRI is still controversial (20–24). An experience similar to the ours concluded that T2*-weighted sequences are mainly helpful for lesion detection but other authors present discordant conclusions (21,24). Our aim was not lesion detection but lesion characterization. Our routine liver protocol does not comprise T2*-weighted sequence due to its low soft-tissue contrast, despite the great sensitivity to magnetic susceptibility. We chose HASTE sequences because they are free-breath, rapid, with high spatial resolution, well reproducible and largely used in clinical practice. Finally, in a preliminary anecdotal study we compared a T2*-weighted sequence with HASTE by the quantitative method. The resultant values, expressed as a percentage (NPSIC,% of SI variation), did not show any significant difference between HASTE and T2*-weighted acquisitions. The difference compared with this previous report (15) is in the lack of normalizing factor in that study.

In our opinion, the greater problem of Resovist in favor of a constant adoption in the daily practice was the inconstant performance in dynamic phases, in particular in arterial acquisition, mainly due to the small quantity of administered CA (maximum 1.4 mL) and then to the little duration time of the arterial contrastographic window, even in the presence of the 20-mL saline flush. Nevertheless, the inconstant contrastographic effect in the arterial phase was ineffective in the total amount of errors in characterization, because the real add-on value of Resovist is at 10-min T2-weighted acquisition, being almost always a complimentary examination, performed after iodinated CT

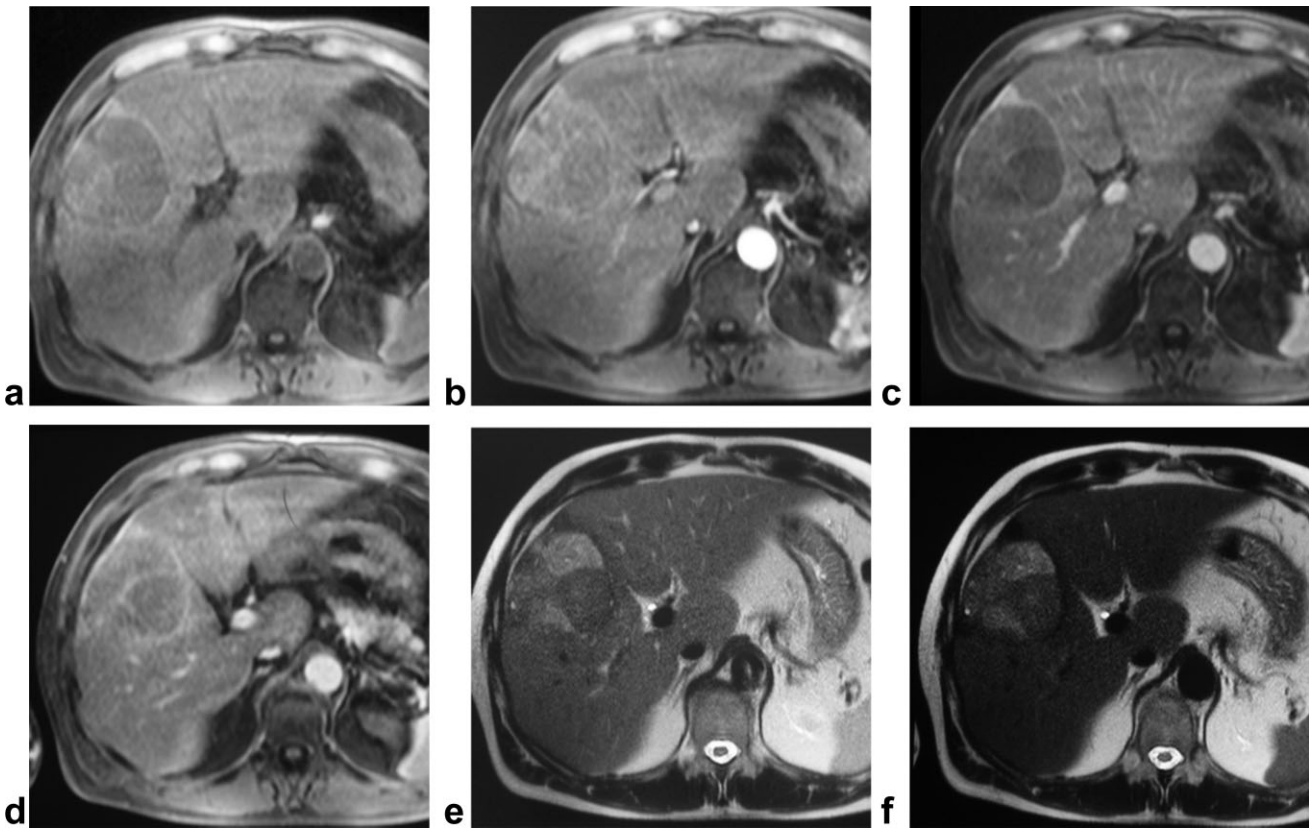


**Figure 5. a–f:** Hepatocellular carcinoma. Unenhanced T1-weighted VIBE acquisition (a) shows a round well-defined hypointense lesion in the V-VIII segment of the liver. After slow bolus Resovist administration, on the hepatic artery phase (b) a slight, heterogeneous enhancement can be detected, with subsequent washout phenomenon on the portal phase (c). At 10-min T1-weighted acquisition a peripheral ring of enhancement is appreciable (d). On the unenhanced HASTE T2-weighted sequence (e), the lesion appears heterogeneously hyper-iso-intense versus surrounding liver parenchyma without any signal intensity change, also at quantitative analysis, on the 10-min contrast-enhanced acquisition (f), where the nodule appears more hyperintense due to the signal loss of the remaining parenchyma.

and/or gadolinium chelates MR studies, both always effective in dynamic phases.

In conclusion, our experience with normalized percentage quantitative evaluation of SI change after slow bolus Resovist administration, allows us to propose the following key points: (i) The main add-on value of quantitative evaluation can be found in late phase-acquisitions; the 10-min T2-weighted sequences permit differentiation of malignant from benign hepatic nodules, while the 10-min T1-weighted sequences

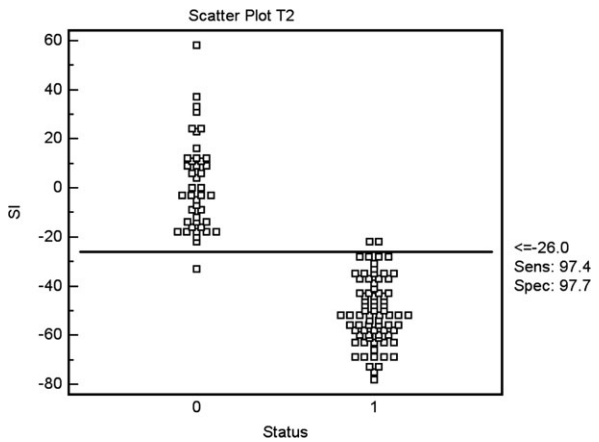


**Figure 6.** Graph-scatter plot T2. Classification of benign (1) versus malignant (0) lesions on T2-weighted images. A cutoff = −26% allowed 97.4% sensitivity and 97.7% specificity.

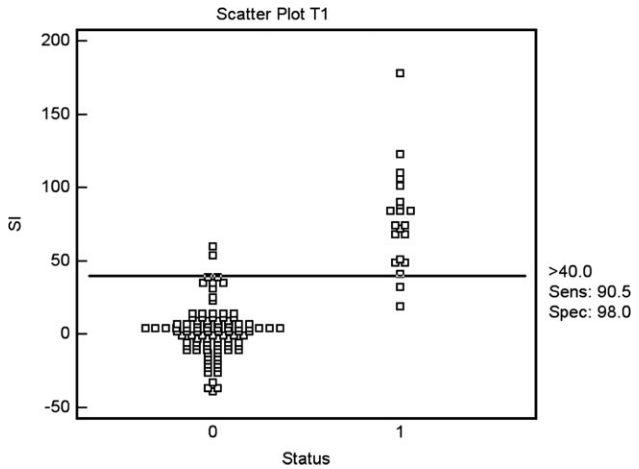


**Figure 7.** Graph-scatter plot T1. Differentiation of hemangioma (1) from all other focal liver lesions (0) on T1-weighted images. A cutoff = +40% permitted 90.5% sensitivity and 98.0% specificity.

distinguish hemangiomas from all other focal liver lesions. (ii) The enhancement obtained on dynamic study seems to be more suitable and confident in hemangiomas and FNHs than in adenomas and HCCs, even if only sometimes comparable with the enhancement induced by liver-specific gadolinium chelates. (iii) This quantitative approach could be useful in classification of a focal liver lesion which is not characterized by liver-specific gadolinium chelates CA.

## REFERENCES


1. Ferrucci JT, Stark DD. Iron oxide-enhanced MR imaging of the liver and spleen: review of the first 5 years. AJR Am J Roentgenol 1990;155:943–950.
2. Kehagias DT, Gouliamos AD, Smyrniotis V, Vlahos LJ. Diagnostic efficacy and safety of MRI of the liver with superparamagnetic iron oxide particles (SHU 555 A). J Magn Reson Imaging 2001; 14:595–601.
3. Shamsi K, Balzer T, Saini S, et al. Superparamagnetic iron oxide particles (SHU 555 A): evaluation of efficacy in three doses for hepatic MR imaging. Radiology 1998;206:365–371.
4. Halavaara JT, Lamminen AE, Bondestam S, Standertskjöld-Nordenstam CG, Hamberg LM. Detection of focal liver lesions with superparamagnetic iron oxide: value of STIR and SE imaging. J Comput Assist Tomogr 1994;18:897–904.
5. Ward J, Chen F, Guthrie JA, et al. Hepatic lesion detection after superparamagnetic iron oxide enhancement: comparison of five T2-weighted sequences at 1.0 T by using alternative-free response receiver operating characteristic analysis. Radiology 2000;214: 159–166.
6. Kondo H, Kanematsu M, Hoshi H, et al. Preoperative detection of malignant hepatic tumors: comparison of combined methods of MR imaging with combined methods of CT. AJR Am J Roentgenol 2000;174:947–954.
7. Hagspiel KD, Neidl KF, Eichenberger AC, Weder W, Marincek B. Detection of liver metastases: comparison of superparamagnetic iron oxide-enhanced and unenhanced MR imaging at 1.5 T with dynamic CT, intraoperative US, and percutaneous US. Radiology 1995;196:471–478.
8. Reimer P, Tombach B. Hepatic MRI with SPIO: detection and characterization of focal liver lesions. Eur Radiol 1998;8:1198–1204.
9. Grazioli L, Morana G, Kirchin MA, et al. MRI of focal nodular hyperplasia (FNH) with gadobenate dimeglumine (Gd-BOPTA) and SPIO (ferumoxides): an intra-individual comparison. J Magn Reson Imaging 2003;17:593–602.
10. Kim YK, Kim CS, Kwak HS, Lee JM. Three-dimensional dynamic liver MR imaging using sensitivity encoding for detection of hepatocellular carcinomas: comparison with superparamagnetic iron oxide-enhanced MR imaging. J Magn Reson Imaging 2004;20: 826–837.
11. Reimer P, Jähnke N, Fiebich M, et al. Hepatic lesion detection and characterization: value of nonenhanced MR imaging, superparamagnetic iron oxide-enhanced MR imaging, and spiral CT-ROC analysis. Radiology 2000;217:152–158.
12. Chen F, Ward J, Robinson PJ. MR imaging of the liver and spleen: a comparison of the effects on signal intensity of two superparamagnetic iron oxide agents. Magn Reson Imaging 1999; 17:549–556.
13. Montet X, Lazeyras F, Howarth N, et al. Specificity of SPIO particles for characterization of liver hemangiomas using MRI. Abdom Imaging 2004;29:60–70.
14. Poeckler-Schoeniger C, Koepke J, Gueckel F, Sturm J, Georgi M. MRI with superparamagnetic iron oxide: efficacy in the detection and characterization of focal hepatic lesions. Magn Reson Imaging 1999;17:383–392.
15. Namkung S, Zech CJ, Helmberger T, Reiser MF, Schoenberg SO. Superparamagnetic iron oxide (SPIO)-enhanced liver MRI with ferucarbotran: efficacy for characterization of focal liver lesions. J Magn Reson Imaging 2007;25:755–765.
16. Schnorr J, Wagner S, Abramjuk C, et al. Focal liver lesions: SPIO, gadolinium, and ferucarbotran-enhanced dynamic T1 weighted and delayed T2-weighted MR imaging in rabbits. Radiology 2006;240:90–100.
17. Wersebe A, Wiskirchen J, Decker U, et al. Comparison of Gadolinium-BOPTA and Ferucarbotran-enhanced three-dimensional T1-weighted dynamic liver magnetic resonance imaging in the same patient. Invest Radiol 2006;41:264–271.
18. Grazioli L, Bondioni MP, Romanini L, et al. Superparamagnetic iron oxide-enhanced liver MRI with SHU 555 A (RESOVIST): new protocol infusion to improve arterial phase evaluation–a prospective study. J Magn Reson Imaging 2009;29:607–616.
19. Lee SW, Park SH, Kim KW, et al. Unenhanced CT for assessment of macrovesicular hepatic steatosis in living liver donors: comparison of visual grading with liver attenuation index. Radiology 2007;244:479–485.
20. Yamamoto H, Yamashita Y, Yoshimatsu S, et al. Hepatocellular carcinoma in cirrhotic livers: detection with unenhanced and iron oxide-enhanced MR imaging. Radiology 1995;195:106–112.
21. Van Beers BE, Lacrosse M, Jamart J, et al. Detection and segmental location of malignant hepatic tumors: comparison of ferumoxides-enhanced gradient-echo and T2-weighted spin-echo MR imaging. AJR Am J Roentgenol 1997;168:713–717.
22. Tang Y, Yamashita Y, Arakawa A, et al. Detection of hepatocellular carcinoma arising in cirrhotic livers: comparison of gadolinium and ferumoxides-enhanced MR imaging. AJR Am J Roentgenol 1999;172:1547–1554.
23. Arbab AS, Ichikawa T, Araki T, et al. Detection of hepatocellular carcinoma and its metastases with various pulse sequences using superparamagnetic iron oxide (SHU-555-A). Abdom Imaging 2000;25:151–158.
24. Kanematsu M, Itoh K, Matsuo M, et al. Malignant hepatic tumor detection with ferumoxides-enhanced MR imaging with a 1.5-T system: comparison of four imaging pulse sequences. J Magn Reson Imaging 2001;13:249–257.